Bis(monoacylglycero)phosphate Promotes Membrane Fusion Facilitated by the SARS-CoV-2 Fusion Domain

Daniel Birtles, Wafa Abbas, Jinwoo Lee*

Department of Chemistry and Biochemistry, University of Maryland, College Park 20742, Maryland, USA

*Email: jinwoo@umd.edu

Abstract

Membrane fusion is a critical component of the viral lifecycle. For SARS-CoV-2, fusion is facilitated by the spike glycoprotein and can take place via either the plasma membrane or endocytic pathway. The fusion domain (FD), which is found within the spike glycoprotein is primarily responsible for the initiation of fusion as it embeds itself within the target cell's membrane. A preference for SARS-CoV-2 to fuse at low pH akin to the environment of endocytic pathway has already been established, however, the impact of the target cell's lipid composition on the FD has yet to be explored. Here we have shown that the SARS-CoV-2 FD preferentially initiates fusion at the late endosomal membrane over the plasma membrane, based upon lipid composition alone. A positive, fusogenic relationship with anionic lipids from the plasma membrane (POPS: 1-palmitoyl-2-oleoyl-sn-glycero-3-phospho-L-serine) and endosomal membrane (BMP: bis(monoacylglycero)phosphate) was established, with a large preference demonstrated for the latter. When comparing the binding affinity and secondary structure of the FD in the presence of different anionic lipids, little deviation was evident whilst the charge was maintained. However, it was discovered that BMP had a subtle, negative impact on lipid packing in comparison to POPS. Furthermore, an inverse relationship between lipid packing and the fusogenecity of the SARS-CoV-2 FD was witnessed. In conclusion, the SARS-CoV-2 FD preferentially initiates fusion at a membrane resembling that of the late endosomal compartment, predominately due to the presence of BMP and its impact on lipid packing.

Introduction

To combat present and emerging viruses we must first understand how they survive on a molecular level. Since the start of the SARS-CoV-2 pandemic, an abundance of research has taken place to enhance our knowledge surrounding the viral lifecycle. This ultimately allowed the rapid innovation of several successful vaccines that eased the global health emergency caused by coronavirus disease 2019 (COVID-19). However, there is still much to learn regarding the underlying molecular mechanisms that make SARS-CoV-2 the extremely infectious virus that it is. One area that is severely lacking is the impact of the target cell's lipid membrane on viral infection, specifically within the process of membrane fusion.

Infection, also referred to as viral entry, begins with receptor binding followed by membrane fusion, with the ultimate goal being the delivery of the viral genome into the target cell. For SARS-CoV-2 this process is facilitated by the spike glycoprotein which consists of two subunits: S1 and S2, responsible for receptor binding and membrane fusion respectively.(1, 2) Initially synthesized as a single precursor, the subunits are cleaved at the S1/S2 site during maturation.(3) This produces the mature spike protein with S1 and S2 held together through non-covalent interactions, ultimately forming a trimeric glycoprotein on the virion surface. To initiate infection, S1 binds the angiotensin converting enzyme 2 (ACE2) receptor on the target cell, leading to S2 being cleaved at a second site (S2') by transmembrane serine protease 2 (TMPRSS2) to enter the cell through the plasma membrane,(4, 5) or endocytosed and later cleaved by cathepsin L.(6, 7) This cleavage event releases the fusion domain (FD; 816-855) at the N-terminus of S2', which embeds itself within the target cells lipid bilayer, perturbing the local membrane environment.(8) Similar roles are thought to be simultaneously carried out by heptad repeat 1 (HR1) and heptad repeat 2 (HR2), on the target and viral membranes respectively.(9) The S2' subunit then refolds into a hairpin-like structure, driven by the formation of the six-helix bundle, with the two membranes pulled into proximity by the anchoring FD and transmembrane domain (TM). During this process, it is thought that the internal fusion peptide (IFP; 867-909) also embeds within the membrane, interacting with both the FD and the TM to complete the fusion process.(10, 11)

Whilst several fusogenic domains in the S2 subunit are integral to the SARS-CoV-2 fusion mechanism, the FD can be considered one of the most crucial membrane-interacting regions. The primary role of a viral FD is to anchor within and perturb the target cell's membrane, serving to initiate the membrane fusion process. Coronaviruses contain a unique FD with two structurally distinct regions that are both required for efficient fusion, implying a novel molecular mechanism.(12-14) The N-terminal portion (S^{816}-F^{833}) is referred to as the fusion peptide (FP) and the C-terminal portion (I^{834}-F^{855}) as the fusion loop (FL), due to their similarity to already established fusogenic regions found in HIV, Influenza and Ebola.(15-17) The importance of the FD to the SARS-CoV-2 lifecycle is further established by the fact that it is 100% conserved across all known variants that have arisen during the pandemic.(18) Combined with high sequence conservation throughout the viral family, these characteristics make the FD a strong therapeutic target for pan-coronavirus inhibition, with several broadly neutralizing antibodies having already been identified.(19, 20)

The exact mechanism by which the SARS-CoV-2 FD initiates membrane fusion becomes even more intriguing when considering that it can utilize both plasma and endosomal membrane pathways for fusion.(21) This is a rather uncommon characteristic for a virus, likely improving the overall success rate of infection. As a result, the FD is expected to embed within two different lipid environments, given that the plasma membrane and endosomal membrane lipid compositions are distinct from one another. In the plasma membrane the predominant lipids are POPC:POPE:POPS:CHOL:SM at an approx. molar ratio of 30:15:5:30:15, whilst the late endosomal membrane contains POPC:POPE:BMP:CHOL:SM at approx. 45:15:20:10:5 (Figure 1A).(22) The remaining 5mol% of both membranes is attributed to 'other' lipids, as a diverse array can be present in the membrane dependent on several environmental factors such as cell type and stress.(23) POPS and BMP are anionic lipids that both contain a single negative charge within their phosphate headgroup. However, due to the rising concentration of BMP as the endocytic pathway progresses, a substantial difference in abundance is present, equating to an approx. four-fold increase in negative charge in the late endosomal membrane when compared to the plasma membrane.(24-26) With this in mind, it comes as no surprise that BMP has been more heavily implicated than POPS in viral fusion,

particularly with viruses that fuse through the endocytic pathway such as Influenza,(27) Lassa Virus (LASV),(28) and Vesicular Stomatitis Virus (VSV).(29) It should be noted that the exact concentration of BMP throughout the endocytic pathway is not certain, though it is established to increase as the pathway progresses, reaching a high of 15-20% in the late endosomal membrane.(22, 24) Another notable difference in the two membrane's lipid compositions is the cholesterol and sphingomyelin content, with both concentrations higher in the plasma membrane.(22) These two lipids are the major constituents of lipid rafts, which are often involved with viral fusion due to receptor localization, however specific impacts on viral FD's have been noted previously.(22, 30-33) Despite the proteins involved in SARS-CoV-2 membrane fusion already having a plethora of research compiled, it is long overdue that the impact of membrane lipids is further investigated to fully understand the fusion process.

In this paper, we found that the SARS-CoV-2 FD more readily elicits fusion with a lipid composition resembling that of the endosomal membrane when compared to the plasma membrane. Moreover, an anionic lipid dependence for FD mediated fusion was discovered, with a significant preference for the endosomal specific lipid BMP. To greater understand the molecular intricacies associated with this preference we carried out a biophysical analysis of how the anionic lipids properties may impact fusion. Despite little variation in binding affinity and secondary structure of the FD amongst different anionic lipids, BMP was discovered to negatively impact lipid packing when compared to POPS. This effect on lipid packing appears to be the main deviation between the two lipids, and due to a negative relationship with the fusogenicity of the FD, could account for the preference for BMP witnessed. Together, the data suggests that the SARS-CoV-2 FD preferentially initiates fusion with a membrane representing the late endosomal membrane, due to the properties conferred by BMP on to the lipid bilayer.

Materials and Methods

Materials

All lipids were acquired from Avanti Polar Lipids in chloroform and their complete chemical names are provided below. POPC: 1-palmitoyl-2-oleoyl-glycero-3-phosphocholine, POPG: 1-palmitoyl-2-oleoyl-sn-glycero-3-phospho-(1'-rac-glycerol), POPS: 1-palmitoyl-2-oleoyl-sn-glycero-3-phospho-L-serine, POPE: 1-palmitoyl-2-oleoyl-sn-glycero-3-phosphoethanolamine, SM: Sphingomyelin, BMP: bis(monooleoylglycero)phosphate (S,R Isomer), DPPC: 1,2-dipalmitoyl-sn-glycero-3-phosphocholine, DOPC: 1,2-dioleoyl-sn-glycero-3-phosphocholine, LissRhod-PE: 1,2-dioleoyl-sn-glycero-3-phosphoethanolamine-N-(lissamine rhodamine B sulfonyl) and NBD-PE: 1,2-dioleoyl-sn-glycero-3-phosphoethanolamine-N-(7-nitro-2-1,3-benzoxadiazol-4-yl). Cholesterol (Chol) was purchased from Anatrace in powder form, then later dissolved with chloroform and aliquoted when needed. C-Laurdan was acquired from Tocris Bioscience, dissolved in DMSO and stored at -80^{o}C.

Preparation of Small and Large Unilamellar Vesicles

Vesicles were assembled from lipid stock solutions in chloroform, with specified amounts added to glass test tubes using Hamilton syringes. The chloroform was then removed by applying a stream of nitrogen whilst gently vortexing the sample to create a lipid film, before being put into a desiccator under vacuum overnight to remove any residual solvent. For large unilamellar vesicles (LUVs), the lipid film was resuspended in 10mM HEPES/MES/Sodium acetate (HMA), 100mM NaCl, pH7.4 buffer through extensive vortexing. When using DPPC, a 5-minute incubation at 55^{o}C prior to vortexing was necessary, due to the lipids transition temperature. The lipid suspensions were then subjected to 10 freeze-thaw cycles between liquid nitrogen and water bath. Liposomes were extruded using a liposofast extrusion kit (Avestin) a total of 21 times through 2 polycarbonate membranes with a 100nm pore size. For small unilamellar vesicles (SUVs), the lipid film was resuspended in the desired buffer and sonicated for 15 mins at 10% duty cycle (1s on/1s off) with the sample sat in ice water, using a Branson ultrasonicator microtip. After sonication the SUVs were centrifuged at 20,000xG for 10mins to remove residual metal particulates. All vesicles were either used immediately or stored for a maximum of 72hrs at 4^{o}C prior to use.

Expression and Purification

The SARS-CoV-2 FD is made up of 40 amino acids (^{816}SFIEDLLFNKVTLADAGFIKQYGDCLGDIAARDLICAQKF^{855}) and designed with an N-terminal 6x His-tag, followed by a SUMO tag to aid with solubility and expression. The expression and purification of the SARS-CoV-2 FD has been described in detail previously.(14) Briefly, 8M urea is used to solubilize the cell pellet followed by Ni-NTA affinity chromatography and cleavage via SUMO protease in dialysis. The cleaved FD is then isolated through the use of Ni-NTA affinity chromatography once again and dialyzed to remove reducing agents, ensuring correct formation of the disulfide bond. Following dialysis, the sample is purified further via a Superdex30 size exclusion chromatography (SEC) column with 10mM HMA 100mM NaCl pH7.4 as the mobile phase. Resulting fractions are pooled, concentration determined via A_{280}, and stored at 4^{o}C.

Circular Dichroism (CD) Spectroscopy

All CD data was acquired via the Jasco J810 Spectro-Polarimeter using a quartz cuvette with a 2mm path length. Each experiment was carried out at room temperature (~22°C) in 1mM HMA, 10mM NaCl, pH7.4 with a protein concentration of ~20μM and a liposome concentration of 800μM. Data was collected from 260nm to 190nm with a step size of 1nm at 20nm/min and averaged over three accumulations. Baselines were acquired without any protein present and subtracted from all data.

Lipid Mixing Assay

LUVs composed of specified lipids were mixed with labelled LUVs containing the same lipid composition as well as 1 mol% of the fluorescent labels: LissRhod-PE and NBD-PE. Experiments were carried out at a ratio of 9:1 unlabeled:labeled in Corning Costar black walled, clear bottom 96 well plates with excitation and emission wavelengths at 460nm and 538nm respectively, with a 530nm cut-off. Fluorescence was recorded using a SpectraMax M5 microplate at room temperature (~22°C). Percent fusion was calculated

as $\frac{(I_F - I_B)}{(I_{100} - I_B)}$, where I_B is the initial background fluorescence, I_F is fluorescence intensity measured after decreasing the pH, and I_{100} is the 100% fluorescence intensity value gathered after complete vesicle rupture following the addition of 1% Triton X-100. All experiments were carried out at pH5.0 unless stated otherwise and contained a peptide/lipid ratio of 0.05 (5μM and 100μM). Controls containing no protein were also ran alongside all conditions, subtracted from the final values and errors propagated from the SEM.

Zeta Potential Measurements

Measurements were acquired on a Horiba Scientific nanoPARTICA Nanoparticle Analyzer SZ-100V2 in a glass capillary cell, with a nominal volume of ~400μL. Each sample was measured in triplicate and the SD is provided. For all pH measurements, a known amount of 1M HCl was added to LUVs in 10mM HMA 100mM NaCl and final values verified via pH meter.

Isothermal Titration Calorimetry (ITC)

The FD sample was prepared through dialysis against 4L of 10mM Sodium Acetate, 100mM NaCl at pH5.0 for 2hrs at 4°C. After this time, the dialysis buffer was used to resuspend the lipid film prior to forming SUVs, with both protein and SUV samples centrifuged at 20,000xG for 10mins, and degassed prior to each experiment. All ITC measurements were taken using a Malvern VP-ITC microcalorimeter with the following experimental parameters in place: initial delay: 2400s, 41 injections (1x2uL and 40x6uL), spacing: 300s, duration: 14.4s, Stir Speed: 270rpm, ref power: 2 μcal/sec and temperature: 22°C. The concentration of the protein sample was taken following dialysis via A_{280}, and the SUV concentration was known from drying down specific volumes of lipid stocks. All processing was conducted through NITPIC and SEDPHAT, with final figures generated through GUSSI.(34) Errors for the simulated fit were generated via Montecarlo analysis within SEDPHAT, with 10,000 iterations and a confidence interval of 0.68.

C-Laurdan Experiments

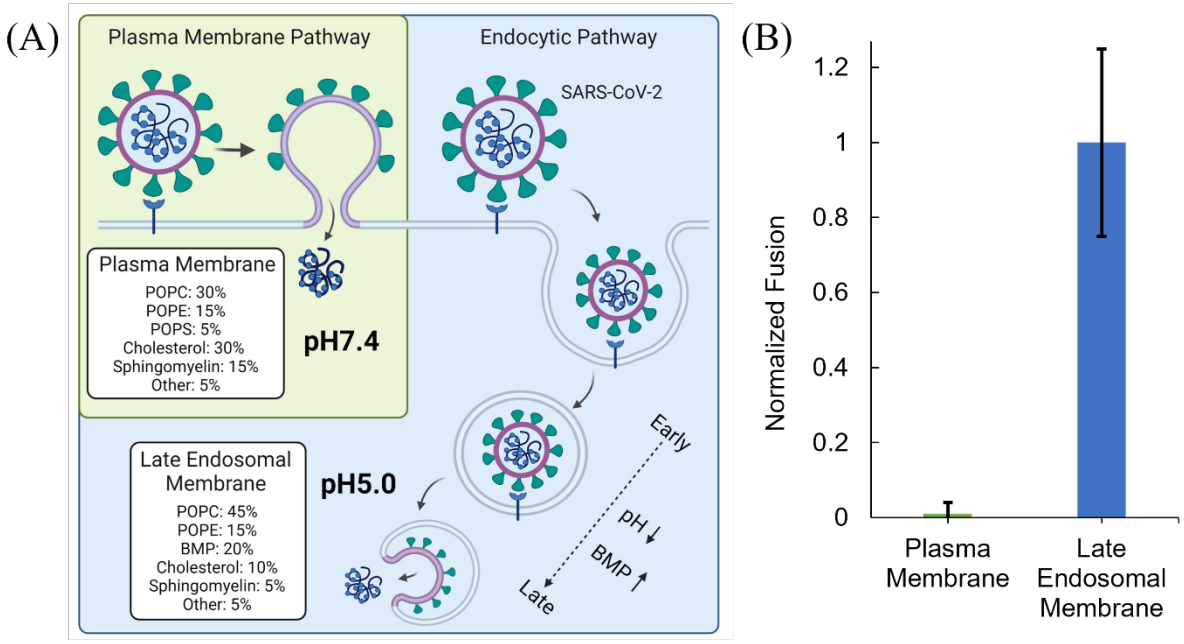

Figure 1: The SARS-CoV-2 FD preferentially initiates fusion with a lipid composition resembling that of the late endosomal membrane. (A) SARS-CoV-2 can enter the target cell via both plasma and endosomal routes. (B) When comparing the fusogenecity of the FD utilizing the respective pH and lipid environments displayed in (A) a clear preference for the late endosomal membrane is observed ($n \leq 4$). The mol% of 'Other' lipids was replaced by POPC in the fusion assay. Created (A) through biorender.com.

All experiments were performed with a C-Laurdan concentration of 500nM, and 100μM of LUVs of a known lipid composition for a final ratio of 1:200. Each composition was run in at least triplicate using a quartz cuvette with a 1cm path length and fluorescence recorded using a SpectraMax M5 microplate at room temperature (~22°C). Excitation wavelength was set to 385nm with the emission spectrum captured from 400-600nm in 2nm steps. Unless stated otherwise, the lipid composition utilized in this assay was 80:20mol% (POPC:Anionic lipid).

Results

With the effect of pH on SARS-CoV-2 FD initiated fusion already established,(12) the next environmental factor to assess was that of the target cells lipid membrane composition. Utilizing an *in vitro* FRET-based fusion assay, the fusogenic ability of the SARS-CoV-2 FD in different physiologically relevant membrane environments has been determined. When presented with a membrane mimicking the plasma or endosomal membrane, we observed a clear and substantial preference for the latter. (Figure 1B) Even when the POPS

content of the plasma membrane mimic is increased to 20mol% and the pH dropped to 5, creating the same net anionic charge and pH environment as seen in the late endosomal membrane, the amount of fusion witnessed is still ~4-fold decreased in comparison. (Figure S1) To better understand this preference, a bottom-up approach was employed to assess whether individual lipids may contribute towards fusion. Interestingly, a significant anionic lipid dependence was observed for both POPS (plasma membrane) and BMP (endosomal membrane), with increasing either lipid resulting in a greater amount of fusion observed (Figure 2A). The role of the negative charge as the primary reason for this positive relationship is corroborated further by the same relationship witnessed with the primarily prokaryotic anionic lipid POPG (Figure S2), as well as two uncharged lipids, POPE and CHOL, having a negative rather than positive impact on fusion (Figure S3). Alongside this general and positive relationship with negatively charged lipids, a specificity for BMP is also apparent through the use of a bias plot that aids in identifying bias towards a given effector molecule (Figure 2B).(35) The graph is generated by plotting the normalized SARS-CoV-2 FD fusion witnessed in BMP membranes against that in POPS, with anionic lipid concentration increasing from left to right. Bias is present if the trajectory does not align with the inserted dashed line and thus, a preference for the FD to initiate fusion with membranes containing BMP over POPS exists. The concentrations of anionic lipids utilized here approximately mimic the increasing concentrations

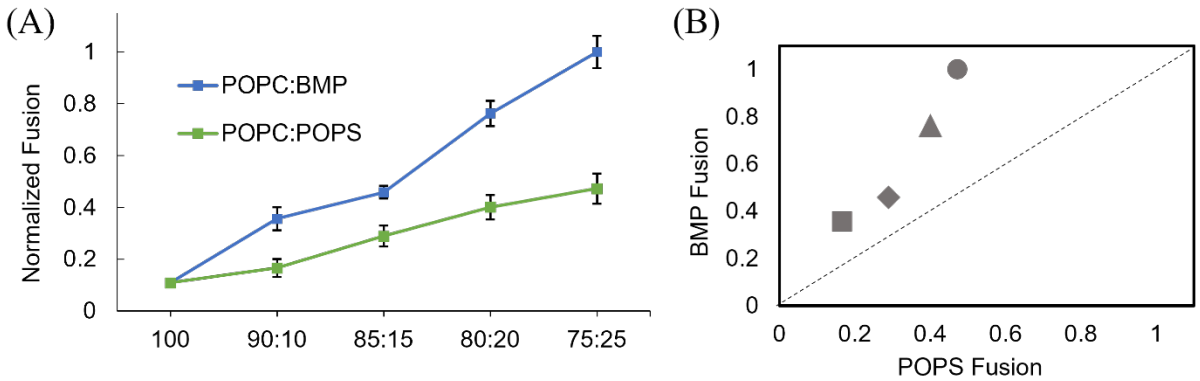

Figure 2: BMP elicits more FD mediated fusion than POPS. (A) When increasing the concentration of anionic lipid present, we observe a positive relationship with fusion for both POPS and BMP, yet more fusion is witnessed for the latter. (B) The bias plot highlights how a specificity for BMP exists and increases alongside anionic lipid concentration. The Y axis represents normalized fusion for BMP, whilst the X axis for POPS. The four data points plotted correspond to the four different anionic lipid concentrations displayed in (A), which are increasing from left to right. ■=10mol%, ♦=15mol%, ▲=20mol%, ●=25mol%. n ≥ 17.

seen throughout the endocytic pathway; intriguingly, the bias plot highlights how the specificity for BMP increases at higher anionic lipid concentrations such as those seen at the late endosomal membrane.

To further probe how different anionic lipids impact the interaction of the FD with the membrane, we quantified the strength of this interaction via isothermal titration calorimetry (ITC) (Figure 3A). A Kd of 1.2 ± 0.1μM, 3.0 ± 0.1μM, and 2.6 ± 0.1μM was found for the FD associating with membranes containing BMP, POPS, and POPG respectively. It should also be noted that the presence of anionic lipids was found to be critical for the interaction between the FD and lipid vesicles, with a ~1000-fold increase in Kd present (4.2 ± 0.7mM) with only POPC in the membrane (Figure S4). Despite being negatively charged at neutral

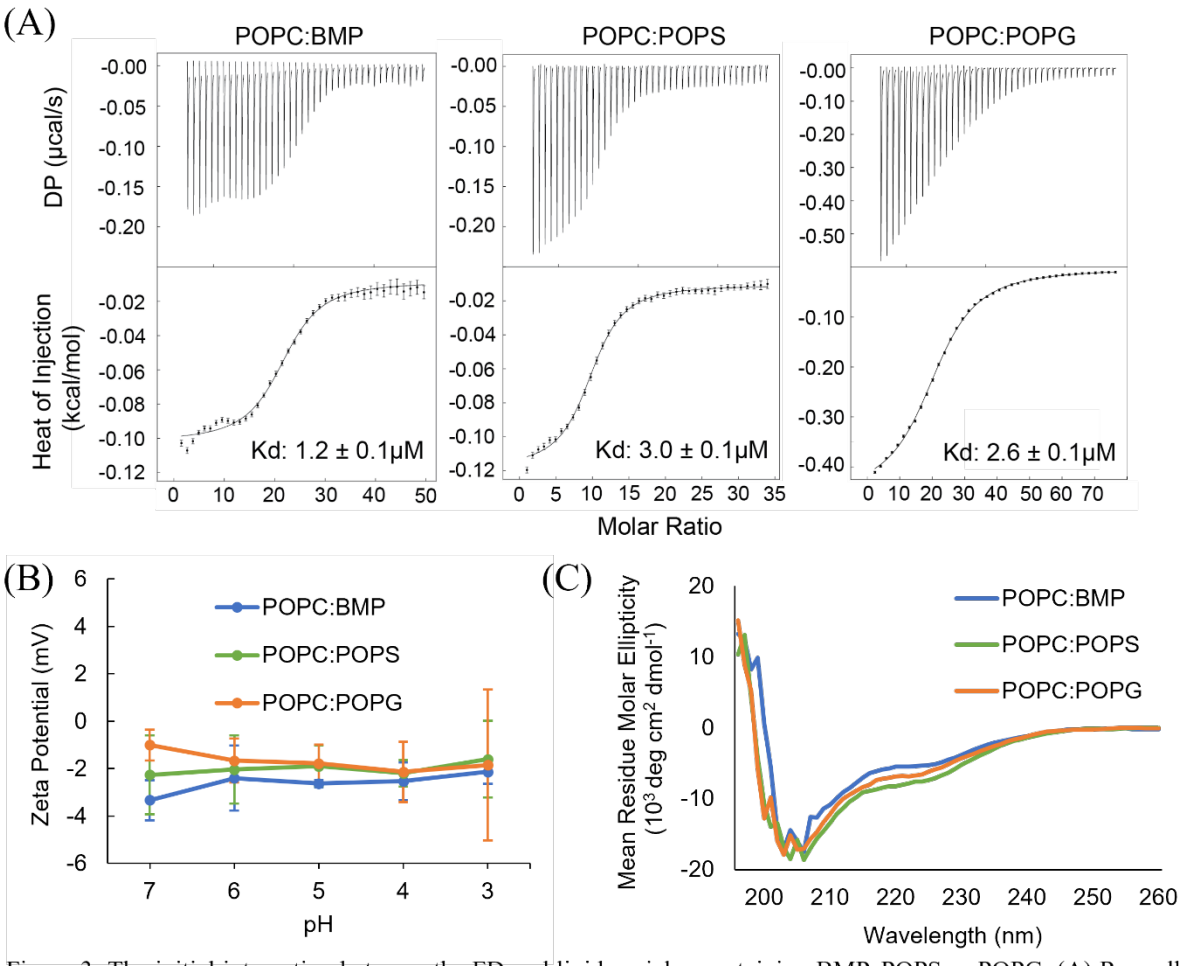

Figure 3: The initial interaction between the FD and lipid vesicles containing BMP, POPS or POPG. (A) Regardless of which anionic lipid is present, the dissociation constants (Kd) found through ITC are similar. Vesicles contained 50mol% anionic lipid with a total concentration of 10mM, and a protein concentration ~20μM was utilized in all ITC experiments. (B) Zeta potential measurements displayed no significant change in charge from pH7 to pH3 with 20mol% anionic lipid present. (C) No major perturbations in global secondary structure were observable via CD based on the presence of different anionic lipids at 20mol%.

pH, it is unknown whether this charge is maintained for all three anionic lipids under more acidic conditions, such as those found in the endocytic pathway. To experimentally probe the relationship between anionic lipid charge and pH we measured the zeta potential of LUVs from pH7.0 to pH3.0. In simplified terms, a zeta potential is the measurement of how the electric potential found to surround a nanoparticle due to the attraction of counterions, changes as the particle moves in solution.(36) By measuring the zeta potentials of LUVs containing BMP, POPS and POPG, we see that no significant alteration in charge occurs for any of the anionic lipids from pH7.0 through to pH3.0 (Figure 3B). Thus, environmental pH does not appear to significantly impact the net negative charge of the constructed lipid vesicles. We also assessed the structural impact of differing anionic lipids on the embedded FD through circular dichroism (CD). An alpha helical conformation for the FD was found in all three lipid environments, as expected based on previous literature (Figure 3C).(14, 37) This suggests that the presence of different lipid headgroups has little impact on the global secondary structure of the FD. Taken together, this data supports a conclusion where a negative charge is essential for the interaction between the SARS-CoV-2 FD and lipid vesicles, however, the different headgroups of the anionic lipids involved has minimal impact on this interaction.

Unable to discern any substantial differences between the anionic lipid headgroups via their interaction with the FD, we next turned our focus to how POPS and BMP may affect the packing of the membrane, and in turn, fusion. C-Laurdan is a fluorescent probe that is sensitive to the local environment and has been used previously to study lipid packing.(38, 39) The probe contains two emission peaks at ~440nm (Increased lipid packing) and ~490nm (Decreased lipid packing), with the relative intensity changing in the presence of different degrees of lipid packing. When first comparing POPC:POPS to POPC:BMP liposomes we see that the presence of POPS results in a slightly more packed membrane, with a λmax of 478nm and 484nm, respectively (Figure 4A&B). To probe this effect further we combined the anionic lipids with DPPC and DOPC, with the hypothesis that they would impact lipid packing based primarily on chain saturation (Figure S5). No change in packing was witnessed for DOPC:BMP (λmax = 484nm), but a minor shift for DOPC:POPS (λmax = 483nm) towards a less packed membrane was observed (Figure S6). Moreover, a clear difference in packing can be seen for both anionic lipids in the presence of

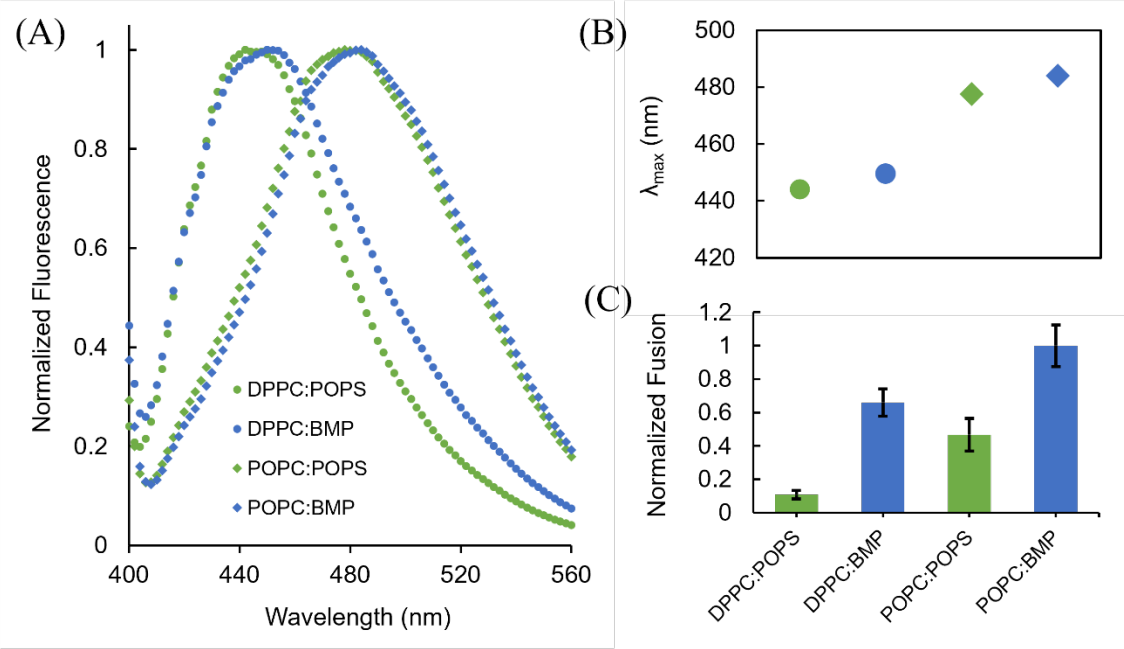

Figure 4: BMP decreases lipid packing, which has a positive impact on fusion. (A) DPPC:POPS and DPPC:BMP show increased lipid packing in comparison to POPC:POPS and POPC:BMP with a molar ratio of 80:20 present. (B) Plotting the lambda max displays a trend where BMP elicits a negative effect on lipid packing in comparison to POPS. (C) When comparing like headgroups, the liposomes containing lower levels of lipid packing allowed the FD to elicit increased amounts of fusion, with a molar ratio of 90:10 and n ≥ 12.

DPPC when compared to POPC (Figure 4A&B). DPPC:POPS (λmax = 444nm) and DPPC:BMP (λmax = 450nm) displayed a marked shift, with a large decrease in λmax indicative of an increase in lipid packing. (Figure 4A&B) Intriguingly, DPPC:BMP still displayed less lipid packing than DPPC:POPS, the same trend as was witnessed with POPC (Figure 4B). Furthermore, a negative relationship was found between increased lipid packing and the fusogenicity of the SARS-CoV-2 FD (Figure 4C). Comparing DPPC:POPS to POPC:POPS and DPPC:BMP to POPC:BMP, an increase in fusion was witnessed with both POPC compositions. In summary, a negative relationship between lipid packing and SARS-CoV-2 FD fusogenecity has been found, with BMP displaying a subtle, negative impact on lipid packing in comparison to POPS.

After assessing the anionic lipids in unison, we finally wanted to investigate whether they displayed any synergistic effects alongside other physiologically relevant lipids. Due to their relatively high abundance in both the plasma and endosomal membranes as well as their previous implications in viral fusion, we focused on POPE and Cholesterol. Intriguingly, the two lipids showed some synergy together

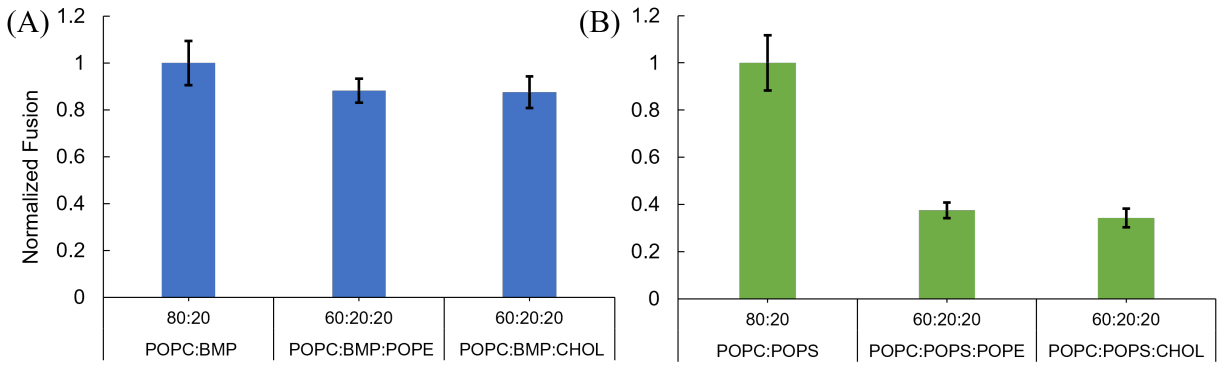

Figure 5: The presence of POPE and cholesterol in the membrane has a negative impact on POPS mediated fusion, but not BMP (A) No difference in fusion is observed with vesicles containing BMP when in the presence of POPE or Cholesterol. (B) FD mediated fusion is significantly decreased when vesicles containing POPS are accompanied with POPE or Cholesterol. $n \leq 10$.

(Figure S7), although at relatively low levels of fusion in comparison to the anionic lipids. When individually incorporating POPE or CHOL into LUVs alongside BMP no significant impact on fusion is observed (Figure 5A). On the other hand, a significant decrease in fusion is witnessed when POPS is incorporated alongside POPE or CHOL (Figure 5B). Hence, whilst neither anionic lipid displays positive synergistic properties alongside POPE or CHOL, both lipids have a detrimental impact on POPS mediated fusion.

Discussion

SARS-CoV-2 is an incredibly infectious virus, in part due to its ability to enter the target cell through either the plasma or endosomal membrane.(4, 40, 41) Whilst most viruses can only access one pathway, the ability to utilize both increases the likelihood of infection. One key difference between the two pathways is environmental pH: the plasma membrane exists at a neutral pH, whilst the pH within the endocytic pathway gradually decreases throughout. Both *in vitro(12)* and *in vivo(41)* SARS-CoV-2 has been shown to preferentially initiate fusion at a pH akin to that witnessed in the endocytic pathway. However, neither study considered the lipid composition of the target cell membrane; another critical environmental factor that differs between the plasma and endosomal routes of fusion. It should be noted that previous work has also found Ca^{2+} to be involved within the initiation of membrane fusion. However, the exact role of Ca^{2+} is yet to be elucidated within this process and we have thus decided to omit the divalent ion from all of our

experiments allowing us to focus on the impact of lipid composition. Here we have shown that the FD of SARS-CoV-2 displays a preference to initiate fusion with the lipid composition found in the late endosomal membrane (Figure 1B), regardless of the environmental pH (Figure S1). Hence, alongside pH, lipid composition could be another major determining factor that dictates the likelihood of success for SARS-CoV-2 fusion.

Within the human body, the sum of POPS (~5mol%) in the plasma membrane is generally thought to be significantly lower than that of BMP (~20mol%) in the late endosomal membrane.(22, 24) Additionally, POPS is thought to be more commonly found on the inner leaflet of the plasma membrane rather than the outer leaflet where it would be exposed to the external environment.(42, 43) So, not only is POPS at a lower concentration than BMP in their respective membranes, but it is also less accessible to interact with the FD. Such reasoning could provide a physiological explanation as to why a preference for the SARS-CoV-2 FD to initiate fusion with membranes containing BMP over POPS exists, as the former is the predominant anionic lipid that comes into contact with the viral glycoprotein (Figure 2). Furthermore, several other viruses which utilize the endocytic pathway (Influenza, LASV, and VSV) have all displayed a positive fusogenic relationships with BMP. (27-29) It is possible that a trend could be emerging, where enveloped viruses which travel through the endocytic pathway take advantage of the increasing concentrations of BMP as a potential trigger to initiate their fusion processes.

We sought to clarify where this preference for BMP arises from by looking at how the anionic lipids impact the membrane from a biophysical perspective. It has previously been stated that BMP elicits fusion in a pH dependent manner,(24) however this was not witnessed within our experimental set-up as controls without FD displayed no fusion regardless of lipid composition (Figure S8). A third anionic lipid was introduced, POPG, which despite being a structural isomer and precursor of BMP retains more similarities with POPS due to headgroup stoichiometry, chain length and saturation.(27) Similarly to POPS, POPG was also not as efficient at eliciting fusion when compared to BMP (Figure S2). Through the use of zeta potential measurements, the overall charge of the lipid membrane was assessed across a wide pH range. The thought process behind these measurements includes the possibility that the negative charge could be

lost as the lipid headgroup becomes protonated at low pH, with the isoelectric points for each functional group not well established. Yet, all three anionic lipids displayed no significant variation between pH7 and pH3, with the negative charge maintained throughout (Figure 3B). Membranes containing BMP, however, were found to be slightly more negative than POPS and POPG. Interestingly, a similar trend was witnessed through ITC, where a slight increase in binding affinity was also discovered for BMP (Figure 3A). We hypothesize that both of these results may be due to a greater preference for BMP to partition into the outer leaflet of LUVs, as the zeta potential measurement only detects the outer surface charge of a given nanoparticle and the FD is only thought to interact with the lipid headgroups of the membranes outer leaflet.(37, 44) Further studies involving the impact of lipid asymmetry may prove beneficial in further elucidating the preference for BMP as well as how the complexity of the membrane impacts fusion. Additionally, the same alpha helical conformation found in previous studies of the FD was also present in all three different lipid environments (Figure 3B). Hence, the FD appears to directly interact with anionic lipids in order to initiate fusion, which explains the positive relationship witnessed. With four positively charged residues within the FD (K825, K835, R847 and K854), an increase in anionic lipid present in the membrane could facilitate more ionic interactions regardless of lipid structure, which based upon the lack of binding for a membrane containing 100mol% POPC, appears critical. However, such interactions do not explain the preference for the FD to fuse at membranes containing BMP over other anionic lipids.

Alongside anionic lipids, both POPE and CHOL have been implicated in viral fusion previously with the lipids found to impact membrane curvature and fluidity, respectively. (45-48) Unexpectedly, neither POPE nor CHOL displayed any positive impact on the ability of the FD to elicit fusion (Figure S3).This was a particular surprise as *in vivo* based studies have shown cholesterol to positively influence SARS-CoV-2 fusion.(49, 50) The discrepancy in results could be due to a greater complexity of membrane lipid compositions involved in such studies, or the more likely scenario, by where the formation of lipid rafts results in the localization of the ACE2 receptor on the cell surface. Hence, rather than direct protein-lipid interactions between the SARS-CoV-2 spike protein and the target cell membrane, it is in fact the membranes impact on the ACE2 receptor that may promote fusion in such cases.

346 The two main characteristics of lipids are a hydrophilic headgroup and two hydrophobic fatty acid
347 tails, both of which play a key role in modulating the biophysical make-up of the membrane.(22, 51, 52)
348 Headgroups often dictate interactions with the soluble environment and are distinguishable by traits such
349 as shape, size and charge. Alternatively, aliphatic chains are more directly involved within the hydrophobic
350 core of the membrane, relying on varying degrees of saturation and length for differentiation. Two key
351 structural differences exist between BMP and POPS which may help to explain the significant differences
352 within fusion, one in the lipid headgroup and another in the fatty acid tails (Figure S5). Firstly, BMP is a
353 structural isomer of phosphatidyl glycerol (PG) that contains a rare sn-1;sn-1' configuration that is not
354 found in any other mammalian glycerophospholipids.(53) This unique configuration has been found to
355 participate in less hydrogen bonding than the traditional sn-3:sn-1' orientation that is found in both POPS
356 and POPG, thought to be due to the orientation of available hydrogen bond donors.(54-56) Secondly, BMP
357 most commonly contains two unsaturated tails (18:1) whilst POPS and POPG have one saturated and one
358 unsaturated chain (16:0-18:1). Saturated fatty acids allow lipids to pack tightly alongside one another,
359 however double bonds introduce kinks to the acyl chains and prevent efficient lipid packing. A simplified
360 example is lipids with saturated acyl chains being thought of as having an overall rectangular shape, so the
361 headgroup and acyl chains are a similar width. Alternatively, unsaturated lipids have a more triangle like
362 shape with their lipid tails consuming a wider area than there headgroup counterpart (Figure S5). Through
363 MD simulations, it has been suggested that the SARS-CoV-2 FD can more readily insert itself into
364 endosomal membranes as opposed to the plasma membrane due to a decrease in lipid packing.(57) Our
365 experimental results further indicate that BMP has a subtle, negative impact on lipid packing when
366 compared to POPS (Figure 4). Put another way, BMP increases the fluidity of the membrane, a finding
367 that has also been corroborated previously,(58) and appears to directly correlate with an increase in fusion
368 elicited by the SARS-CoV-2 FD (Figure 4C). Increasing polyunsaturated lipids in the membrane has been
369 shown to favor fusion through decreasing the overall activation energy required previously.(59) Thus,
370 greater membrane fluidity via the presence of BMP as a result of less hydrogen bonding and increased
371 unsaturation, could aid the FD in reducing the energetic barrier necessary to elicit fusion.

Conclusions

The SARS-CoV-2 FD contains a preference to elicit fusion in membranes containing the endosomal lipid BMP. Alongside its negative charge, which is maintained across a wide pH range encompassing the endosomal pathway, BMP is thought to have a subtle, negative impact lipid packing, likely due to its unique structural characteristics. Together, these properties are deemed to be critical for the positive and specific impact on membrane fusion witnessed when BMP is compared to POPS. The negative charge shared by both lipids is critical for the initial interaction between the FD and the lipid membrane, whilst the minor decrease in lipid packing imparted by BMP results in increased FD mediated fusion. Intriguingly, whilst fusion with membranes containing POPS was negatively impacted by the presence of POPE or cholesterol, BMP showed neither positive nor negative synergistic effects alongside other lipids (Figure 5). Further work should prioritize understanding the interplay of such lipids within the membrane and how that may directly impact SARS-CoV-2 mediated fusion in more complex systems incorporating features such as lipid asymmetry and phase separation. This knowledge could be applied to other viruses, aiding in the understanding of viral tropism through different membrane lipid compositions.

Supporting Information

S1. The impact on fusion when matching the anionic lipid concentration and pH in the plasma membrane to that of the endosomal membrane

S2. Positive relationship between POPG concentration and SARS-CoV-2 FD mediated fusion

S3. Impact of POPE and cholesterol on SARS-CoV-2 FD mediated fusion

S4. SARS-CoV-2 FD binding to 100% POPC vesicles

S5. Chemical structures of POPC, DOPC, DPPC, POPG, POPS and BMP lipids.

S6. Lipid packing of DOPC:POPS v DOPC:BMP

S7. Synergistic relationship witnessed with POPE and cholesterol

S8. Control data for fusion experiments with anionic lipids and general data processing work flow

Acknowledgements

We would like to thank Oluwatobi Aderotoye and Dr. Sung Joon Kim at Howard University for the use of their Horiba Scientific nanoPARTICA Nanoparticle Analyzer SZ-100V2 used to acquire the zeta potential data displayed within this manuscript. Also a special thanks to the rest of the Lee Lab for their helpful comments and discussions in constructing this manuscript.

Funding Sources

This work was supported by the University of Maryland – College Park and the National Science Foundation, Division of Chemistry (CHE: 2238139).

References

(1) Wang, Q.; Zhang, Y.; Wu, L.; Niu, S.; Song, C.; Zhang, Z.; Lu, G.; Qiao, C.; Hu, Y.; Yuen, K. Y.; et al. Structural and Functional Basis of SARS-CoV-2 Entry by Using Human ACE2. *Cell* **2005**, *181* (4), 894-904. DOI: 10.1016/j.cell.2020.03.045.

(2) Simmons, G.; Reeves, J. D.; Rennekamp, A. J.; Amberg, S. M.; Piefer, A. J.; Bates, P. Characterization of severe acute respiratory syndrome-associated coronavirus (SARS-CoV) spike glycoprotein-mediated viral entry. *Proc Natl Acad Sci U S A* **2004**, *101* (12), 4240-4245. DOI: 10.1073/pnas.0306446101.

(3) Belouzard, S.; Chu, V. C.; Whittaker, G. R. Activation of the SARS coronavirus spike protein via sequential proteolytic cleavage at two distinct sites. *Proc Natl Acad Sci U S A* **2009**, *106* (14), 5871-5876. DOI: 10.1073/pnas.0809524106.

(4) Hoffmann, M.; Kleine-Weber, H.; Schroeder, S.; Krüger, N.; Herrler, T.; Erichsen, S.; Schiergens, T. S.; Herrler, G.; Wu, N.-H.; Nitsche, A.; et al. SARS-CoV-2 Cell Entry Depends on ACE2 and TMPRSS2 and Is Blocked by a Clinically Proven Protease Inhibitor. *Cell* **2020**, *181* (2), 271-280.e278. DOI: 10.1016/j.cell.2020.02.052 (acccessed 2021-02-01T19:31:27).

(5) Matsuyama, S.; Nagata, N.; Shirato, K.; Kawase, M.; Takeda, M.; Taguchi, F. Efficient Activation of the Severe Acute Respiratory Syndrome Coronavirus Spike Protein by the Transmembrane Protease TMPRSS2. *J Virol.* **2010**, *84* (24), 12658-12664. DOI: 10.1128/JVI.01542-10.

(6) Bollavaram, K.; Leeman, T. H.; Lee, M. W.; Kulkarni, A.; Upshaw, S. G.; Yang, J.; Song, H.; Platt, M. O. Multiple sites on SARS-CoV-2 spike protein are susceptible to proteolysis by cathepsins B, K, L, S, and V. *Protein Sci* **2021**, *30* (6), 1131-1143. DOI: 10.1002/pro.4073.
(7) Simmons, G.; Gosalia, D. N.; Rennekamp, A. J.; Reeves, J. D.; Diamond, S. L.; Bates, P. Inhibitors of cathepsin L prevent severe acute respiratory syndrome coronavirus entry. *Proc Natl Acad Sci U S A* **2005**, *102* (33), 11876-11881. DOI: 10.1073/pnas.0505577102.
(8) Lai, A. L.; Freed, J. H. SARS-CoV-2 Fusion Peptide has a Greater Membrane Perturbating Effect than SARS-CoV with Highly Specific Dependence on Ca2+. *J Mol Biol* **2021**, *433* (10), 166946. DOI: 10.1016/j.jmb.2021.166946. (acccessed 2021-02-10T19:40:35).
(9) Chiliveri, S. C.; Louis, J. M.; Ghirlando, R.; Bax, A. Transient lipid-bound states of spike protein heptad repeats provide insights into SARS-CoV-2 membrane fusion. *Sci Adv* **2021**, *7* (41), eabk2226. DOI: 10.1126/sciadv.abk2226.
(10) Birtles, D.; Lee, J. SARS-CoV-2 Fusion Domain Provides Clues toward the Molecular Mechanism for Membrane Fusion. *Biochemistry* **2023**, 62, 3033–3035. DOI: 10.1021/acs.biochem.3c00501.
(11) Shi, W.; Cai, Y.; Zhu, H.; Peng, H.; Voyer, J.; Rits-Volloch, S.; Cao, H.; Mayer, M. L.; Song, K.; Xu, C.; et al. Cryo-EM structure of SARS-CoV-2 postfusion spike in membrane. *Nature* **2023**, *619* (7969), 403-409. DOI: 10.1038/s41586-023-06273-4
(12) Birtles, D.; Oh, A. E.; Lee, J. Exploring the pH dependence of the SARS-CoV-2 complete fusion domain and the role of its unique structural features. *Protein Science* **2022**, *31* (9), e4390. DOI: 10.1002/pro.4390
(13) Lai, A. L.; Millet, J. K.; Daniel, S.; Freed, J. H.; Whittaker, G. R. The SARS-CoV Fusion Peptide Forms an Extended Bipartite Fusion Platform That Perturbs Membrane Order in a Calcium-Dependent Manner. *J Mol Biol* **2017**, *429* (24), 3875-3892. DOI: 10.1016/j.jmb.2017.10.017.
(14) Birtles, D.; Lee, J.. Identifying Distinct Structural Features of the Sars-cov-2 Spike Protein Fusion Domain Essential for Membrane Interaction. Biochemistry **2021**, 60 (40), 2978–2986. https://doi.org/10.1021/acs.biochem.1c00543.
(15) Dimitrov, A. S.; Rawat, S. S.; Jiang, S.; Blumenthal, R. Role of the Fusion Peptide and Membrane-Proximal Domain in HIV-1 Envelope Glycoprotein-Mediated Membrane Fusion. *Biochemistry* **2003**, *42* (48), 14150-14158. DOI: 10.1021/bi035154g
(16) Han, X.; Bushweller, J. H.; Cafiso, D. S.; Tamm, L. K. Membrane structure and fusion-triggering conformational change of the fusion domain from influenza hemagglutinin. *Nature Structural Biology* **2001**, *8* (8), 715-720. DOI: 10.1038/90434
(17) Gregory, S. M.; Harada, E.; Liang, B.; Delos, S. E.; White, J. M.; Tamm, L. K. Structure and function of the complete internal fusion loop from Ebolavirus glycoprotein 2. *Proc Natl Acad Sci U S A* **2011**, *108* (27), 11211-11216. DOI: 10.1073/pnas.1104760108.
(18) *CoVariants*. **2024**. https://covariants.org (Date accessed: 09.20.2023)
(19) Low, J. S.; Jerak, J.; Tortorici, M. A.; Mccallum, M.; Pinto, D.; Cassotta, A.; Foglierini, M.; Mele, F.; Abdelnabi, R.; Weynand, B.; et al. ACE2-binding exposes the SARS-CoV-2 fusion peptide to broadly neutralizing coronavirus antibodies. *Science* **2022**, *377* (6607), 735-742. DOI: 10.1126/science.abq2679
(20) Dacon, C.; Tucker, C.; Peng, L.; Lee, C. D.; Lin, T. H.; Yuan, M.; Cong, Y.; Wang, L.; Purser, L.; Williams, J. K.; et al. Broadly neutralizing antibodies target the coronavirus fusion peptide. *Science* **2022**, *377* (6607), 728-735. DOI: 10.1126/science.abq3773.
(21) Hoffmann, M.; Kleine-Weber, H.; Pöhlmann, S. A Multibasic Cleavage Site in the Spike Protein of SARS-CoV-2 Is Essential for Infection of Human Lung Cells. *Mol Cell* **2020**, *78* (4), 779-784.e775. DOI: 10.1016/j.molcel.2020.04.022.
(22) Van Meer, G.; Voelker, D. R.; Feigenson, G. W. Membrane lipids: where they are and how they behave. *Nature Reviews Molecular Cell Biology* **2008**, *9* (2), 112-124. DOI: 10.1038/nrm2330
(23) Symons, J. L.; Cho, K.-J.; Chang, J. T.; Du, G.; Waxham, M. N.; Hancock, J. F.; Levental, I.; Levental, K. R. Lipidomic atlas of mammalian cell membranes reveals hierarchical variation induced by culture

conditions, subcellular membranes, and cell lineages. *Soft Matter* **2021**, *17* (2), 288-297. DOI: 10.1039/d0sm00404a
(24) Kobayashi, T.; Beuchat, M. H.; Chevallier, J.; Makino, A.; Mayran, N.; Escola, J. M.; Lebrand, C.; Cosson, P.; Gruenberg, J. Separation and characterization of late endosomal membrane domains. *J Biol Chem* **2002**, *277* (35), 32157-32164. DOI: 10.1074/jbc.M202838200.
(25) Kobayashi, T.; Beuchat, M.-H.; Lindsay, M.; Frias, S.; Palmiter, R. D.; Sakuraba, H.; Parton, R. G.; Gruenberg, J. Late endosomal membranes rich in lysobisphosphatidic acid regulate cholesterol transport. *Nature Cell Biology* **1999**, *1* (2), 113-118. DOI: 10.1038/10084
(26) Kobayashi, T.; Stang, E.; Fang, K. S.; De Moerloose, P.; Parton, R. G.; Gruenberg, J. A lipid associated with the antiphospholipid syndrome regulates endosome structure and function. *Nature* **1998**, *392* (6672), 193-197. DOI: 10.1038/32440
(27) Mannsverk, S.; Villamil Giraldo, A. M.; Kasson, P. M. Influenza Virus Membrane Fusion Is Promoted by the Endosome-Resident Phospholipid Bis(monoacylglycero)phosphate. *The Journal of Physical Chemistry B* **2022**, *126* (49), 10445-10451. DOI: 10.1021/acs.jpcb.
(28) Markosyan, R. M.; Marin, M.; Zhang, Y.; Cohen, F. S.; Melikyan, G. B. The late endosome-resident lipid bis(monoacylglycero)phosphate is a cofactor for Lassa virus fusion. *PLOS Pathogens* **2021**, *17* (9), e1009488. DOI: 10.1371/journal.ppat.1009488
(29) Roth, S. L.; Whittaker, G. R. Promotion of vesicular stomatitis virus fusion by the endosome-specific phospholipid bis(monoacylglycero)phosphate (BMP). *FEBS Letters* **2011**, *585* (6), 865-869. DOI: 10.1016/j.febslet.2011.02.015
(30) Silvius, J. R. Role of cholesterol in lipid raft formation: lessons from lipid model systems. *Biochim Biophys Acta* **2003**, *1610* (2), 174-183. DOI: 10.1016/s0005-2736(03)00016-6.
(31) Kulkarni, R.; Wiemer, E. A. C.; Chang, W. Role of Lipid Rafts in Pathogen-Host Interaction - A Mini Review. *Front Immunol* **2021**, *12*, 815020. DOI: 10.3389/fimmu.2021.815020.
(32) Yang, S.-T.; Kiessling, V.; Simmons, J. A.; White, J. M.; Tamm, L. K. HIV gp41–mediated membrane fusion occurs at edges of cholesterol-rich lipid domains. *Nature Chemical Biology* **2015**, *11* (6), 424-431. DOI: 10.1038/nchembio.1800
(33) Lai, A. L.; Moorthy, A. E.; Li, Y.; Tamm, L. K. Fusion activity of HIV gp41 fusion domain is related to its secondary structure and depth of membrane insertion in a cholesterol-dependent fashion. *J Mol Biol* **2012**, *418* (1-2), 3-15. DOI: 10.1016/j.jmb.2012.02.010.
(34) Zhao, H.; Piszczek, G.; Schuck, P. SEDPHAT – A platform for global ITC analysis and global multi-method analysis of molecular interactions. *Methods* **2015**, *76*, 137-148. DOI: 10.1016/j.ymeth.2014.11.012 (acccessed 2023-10-16T20:12:35).
(35) Karl, K.; Paul, M. D.; Pasquale, E. B.; Hristova, K. Ligand bias in receptor tyrosine kinase signaling. *Journal of Biological Chemistry* **2020**, *295* (52), 18494-18507. DOI: 10.1074/jbc.rev120.015190
(36) Clogston, J. D.; Patri, A. K. Zeta Potential Measurement. In *Methods in Molecular Biology*, Humana Press, 2011; pp 63-70.
(37) Koppisetti, R. K.; Fulcher, Y. G.; Van Doren, S. R. Fusion Peptide of SARS-CoV-2 Spike Rearranges into a Wedge Inserted in Bilayered Micelles. *Journal of the American Chemical Society* **2021**, *143* (33), 13205-13211. DOI: 10.1021/jacs.1c05435
(38) Sezgin, E.; Sadowski, T.; Simons, K. Measuring Lipid Packing of Model and Cellular Membranes with Environment Sensitive Probes. *Langmuir* **2014**, *30* (27), 8160-8166. DOI: 10.1021/la501226v
(39) Kim, H. M.; Choo, H. J.; Jung, S. Y.; Ko, Y. G.; Park, W. H.; Jeon, S. J.; Kim, C. H.; Joo, T.; Cho, B. R. A Two-Photon Fluorescent Probe for Lipid Raft Imaging: C-Laurdan. *ChemBioChem* **2007**, *8* (5), 553-559. DOI: 10.1002/cbic.200700003
(40) Zhou, T.; Tsybovsky, Y.; Gorman, J.; Rapp, M.; Cerutti, G.; Chuang, G. Y.; Katsamba, P. S.; Sampson, J. M.; Schön, A.; Bimela, J.; et al. Cryo-EM Structures of SARS-CoV-2 Spike without and with ACE2 Reveal a

pH-Dependent Switch to Mediate Endosomal Positioning of Receptor-Binding Domains. *Cell Host Microbe* **2020**, *28* (6), 867-879.e865. DOI: 10.1016/j.chom.2020.11.004.
(41) Kreutzberger, A. J. B.; Sanyal, A.; Saminathan, A.; Bloyet, L.-M.; Stumpf, S.; Liu, Z.; Ojha, R.; Patjas, M. T.; Geneid, A.; Scanavachi, G.; et al. SARS-CoV-2 requires acidic pH to infect cells. *Proceedings of the National Academy of Sciences* **2022**, *119* (38), e2209514119. DOI: 10.1073/pnas.2209514119
(42) Bretscher, M. S. Asymmetrical Lipid Bilayer Structure for Biological Membranes. *Nature New Biology* **1972**, *236* (61), 11-12. DOI: 10.1038/newbio236011a0
(43) Op Den Kamp, J. A. F. Lipid Asymmetry in Membranes. *Annual Review of Biochemistry* **1979**, *48* (1), 47-71. DOI: 10.1146/annurev.bi.48.070179.000403
(44) Van Doren, S. R.; Scott, B. S.; Koppisetti, R. K. SARS-CoV-2 fusion peptide sculpting of a membrane with insertion of charged and polar groups. *Structure* **2023**, *31* (10), 1184-1199.e1183. DOI: 10.1016/j.str.2023.07.015.
(45) Lee, J.; Kreutzberger, A. J. B.; Odongo, L.; Nelson, E. A.; Nyenhuis, D. A.; Kiessling, V.; Liang, B.; Cafiso, D. S.; White, J. M.; Tamm, L. K. Ebola virus glycoprotein interacts with cholesterol to enhance membrane fusion and cell entry. *Nature Structural & Molecular Biology* **2021**, *28* (2), 181-189. DOI: 10.1038/s41594-020-00548-4
(46) Qiang, W.; Sun, Y.; Weliky, D. P. A strong correlation between fusogenicity and membrane insertion depth of the HIV fusion peptide. *Proc Natl Acad Sci U S A* **2009**, *106* (36), 15314-15319. DOI: 10.1073/pnas.0907360106.
(47) Biswas, S.; Yin, S.-R.; Blank, P. S.; Zimmerberg, J. Cholesterol Promotes Hemifusion and Pore Widening in Membrane Fusion Induced by Influenza Hemagglutinin. *Journal of General Physiology* **2008**, *131* (5), 503-513. DOI: 10.1085/jgp.200709932
(48) Lee, M.; Morgan, C. A.; Hong, M. Fully hydrophobic HIV gp41 adopts a hemifusion-like conformation in phospholipid bilayers. *J Biol Chem* **2019**, *294* (40), 14732-14744. DOI: 10.1074/jbc.RA119.009542.
(49) Niort, K.; Dancourt, J.; Boedec, E.; Al Amir Dache, Z.; Lavieu, G.; Tareste, D. Cholesterol and Ceramide Facilitate Membrane Fusion Mediated by the Fusion Peptide of the SARS-CoV-2 Spike Protein. *ACS Omega* **2023**, *8* (36), 32729-32739. DOI: 10.1021/acsomega.3c03610
(50) Sanders, D. W.; Jumper, C. C.; Ackerman, P. J.; Bracha, D.; Donlic, A.; Kim, H.; Kenney, D.; Castello-Serrano, I.; Suzuki, S.; Tamura, T.; et al. SARS-CoV-2 requires cholesterol for viral entry and pathological syncytia formation. *eLife* **2021**, *10*, e65962. DOI: 10.7554/elife.65962
(51) Ding, W.; Palaiokostas, M.; Wang, W.; Orsi, M. Effects of Lipid Composition on Bilayer Membranes Quantified by All-Atom Molecular Dynamics. *The Journal of Physical Chemistry B* **2015**, *119* (49), 15263-15274. DOI: 10.1021/acs.jpcb.5b06604
(52) Ballweg, S.; Sezgin, E.; Doktorova, M.; Covino, R.; Reinhard, J.; Wunnicke, D.; Hänelt, I.; Levental, I.; Hummer, G.; Ernst, R. Regulation of lipid saturation without sensing membrane fluidity. *Nature Communications* **2020**, *11* (1), 14528-1. DOI: 10.1038/s41467-020-14528-1
(53) Akgoc, Z.; Sena-Esteves, M.; Martin, D. R.; Han, X.; D'Azzo, A.; Seyfried, T. N. Bis(monoacylglycero)phosphate: a secondary storage lipid in the gangliosidoses. *Journal of Lipid Research* **2015**, *56* (5), 1005-1006. DOI: 10.1194/jlr.m057851
(54) Hayakawa, T.; Hirano, Y.; Makino, A.; Michaud, S.; Lagarde, M.; Pageaux, J.-F.; Doutheau, A.; Ito, K.; Fujisawa, T.; Takahashi, H.; et al. Differential Membrane Packing of Stereoisomers of Bis(monoacylglycero)phosphate. *Biochemistry* **2006**, *45* (30), 9198-9209. DOI: 10.1021/bi060722o
(55) Dickey, A.; Faller, R. Examining the Contributions of Lipid Shape and Headgroup Charge on Bilayer Behavior. *Biophysical Journal* **2008**, *95* (6), 2636-2646. DOI: 10.1529/biophysj.107.128074
(56) Mukhopadhyay, P.; Monticelli, L.; Tieleman, D. P. Molecular Dynamics Simulation of a Palmitoyl-Oleoyl Phosphatidylserine Bilayer with Na+ Counterions and NaCl. *Biophysical Journal* **2004**, *86* (3), 1601-1609. DOI: 10.1016/s0006-3495(04)74227-7

(57) Schaefer, S. L.; Jung, H.; Hummer, G. Binding of SARS-CoV-2 Fusion Peptide to Host Endosome and Plasma Membrane. *J Phys Chem B* **2021**, *125* (28), 7732-7741. DOI: 10.1021/acs.jpcb.1c04176.
(58) Holopainen, J. M.; Söderlund, T.; Alakoskela, J. M.; Säily, M.; Eriksson, O.; Kinnunen, P. K. Intermolecular interactions of lysobisphosphatidic acid with phosphatidylcholine in mixed bilayers. *Chem Phys Lipids* **2005**, *133* (1), 51-67. DOI: 10.1016/j.chemphyslip.2004.08.004.
(59) François-Martin, C.; Bacle, A.; Rothman, J. E.; Fuchs, P. F. J.; Pincet, F. Cooperation of Conical and Polyunsaturated Lipids to Regulate Initiation and Processing of Membrane Fusion. *Front Mol Biosci* **2021**, *8*, 763115. DOI: 10.3389/fmolb.2021.763115.

For Table Of Contents Only